




Cite this: *RSC Adv.*, 2017, 7, 29540

Dual temperature- and pH-responsive polymeric micelle for selective and efficient two-step doxorubicin delivery†

Yuki Hiruta, * Yuki Kanda, Naoya Katsuyama and Hideko Kanazawa*‡

We report a polymeric micelle drug delivery system, which enables selective intracellular uptake with external thermal stimulation, and effective release of a drug at internal acidic endosomal pH. We developed a dual temperature- and pH-responsive polymeric micelle composed of a temperature-responsive corona segment with poly(*N*-isopropylacrylamide-*co*-dimethylacrylamide) [P(NIPAAm-*co*-DMAAm)] and a pH-responsive core segment with poly[2-(diisopropylamino)ethyl methacrylate] (PDPA). A dual temperature- and pH-responsive amphiphilic diblock copolymer was synthesized by reversible addition–fragmentation chain transfer (RAFT) polymerization. The dithiobenzoate end-group was removed with radical-induced ester exchange. This copolymer formed nano-sized micelles in aqueous solution, and encapsulated anti-cancer agent, doxorubicin (DOX). The resultant micelles exhibited a temperature-dependent phase transition at a temperature slightly higher than body temperature, and intracellular uptake of encapsulated DOX was accelerated above the phase transition temperature. A transition from neutral to positive charge, leading to micelle disassembly, accelerated the release of Nile red as a model drug. The cytotoxicity of doxorubicin (DOX)-loaded dual temperature- and pH-responsive micelles against human cervical cancer HeLa cells was significantly greater at 42 °C than at 37 °C, while no significant temperature-dependent cytotoxicity was observed with DOX-loaded micelles that were only temperature-responsive. This proof-of-concept synergistic two-step delivery system with enhanced intracellular uptake upon external thermal stimulation and rapid release of DOX at internal acidic endosomal pH was effective against tumor cells *in vitro*.

Received 28th March 2017
 Accepted 31st May 2017

DOI: 10.1039/c7ra03579a

rsc.li/rsc-advances

Introduction

Nanomedicines such as micelles, liposomes, and particles with an enhanced permeation and retention (EPR) effect are effective for tumor chemotherapy.^{1,2} Polyethylene glycol (PEG) contributed to the development of nanomedicines,^{3,4} as its incorporation onto their surface prolongs their circulation in the bloodstream after intravenous administration. However, PEG prevents intracellular uptake and endosomal escape, which results in the loss of drug activity. These issues regarding the use of PEG for tumor drug delivery are referred to as the “PEG dilemma”.^{5,6} A variety of strategies were studied to overcome these drawbacks. One of these strategies is the modification of the end-group of the PEG segment with ligands such as folate,⁷

cyclic Arg–Gly–Asp (cRGD) peptide,⁸ and antibody fragments⁹ that recognize cell-specific surface receptors, leading to the improvement of cellular selectivity and increased intracellular delivery of nanomedicines. Stimuli-responsive polymers or “smart materials”,¹⁰ whose characteristics undergo appropriate changes in response to surrounding environmental conditions,^{11–14} were also studied for tumor targeting and effective release of anti-tumor agents.¹⁵

Hyperthermia, a procedure during which localized tumor tissue is heated to 40–43 °C, can synergistically enhance tumor cytotoxicity when combined with chemotherapy.¹⁶ Besides the therapeutic effect of hyperthermia, temperature-responsive polymers, which exhibited reversible temperature-dependent hydrophilic/hydrophobic phase transition, were applied to a drug carrier for a stimuli-responsive targeting.^{17,18} When this system was applied to *in vivo* systems, temperature-responsive polymer accumulated to local heated tissue as aggregation and precipitation. In some cases, the polymer aggregate were sheared from local heated tissue, and carried away by the blood flow. Some polymeric micelles washed from the local heated tissue would be expected to rapidly disaggregate, and recovery its hydrophilic corona due to reversible temperature-responsive characteristic.¹⁹ The tumor extracellular microenvironment

Faculty of Pharmacy, Keio University, 1-5-30 Shibakoen, Minato, Tokyo 105-8512, Japan. E-mail: hiruta@applc.keio.ac.jp; kanazawa-hd@pha.keio.ac.jp; Fax: +81-3-5400-1378; Tel: +81-3-5400-2657

† Electronic supplementary information (ESI) available: Cell viabilities, and ¹H NMR spectra of polymers. See DOI: 10.1039/c7ra03579a

‡ Present address: Department of Applied Chemistry, Faculty of Science and Technology, Keio University, 3-14-1, Hiyoshi, Kohoku-ku, Yokohama 223-8522, Japan.



exhibits acidic pH values (pH_e : $pH \sim 6.8$) due to the high rate of glycolysis in tumor cells resulted in high lactic acid levels of extracellular microenvironment, both in aerobic and anaerobic conditions.²⁰ Intracellular endo/lysosome are an acidic organelle (pH_i : $pH 5.0-6.0$).²¹ These different pH values are focus of attention for efficient anti-tumor drug delivery with pH responsive materials. Various pH-responsive nanomedicines have been developed for efficient drug delivery.²² Furthermore, dual stimuli responsive nanomedicines in response to an internal or external stimulus, such as dual pH,^{23,24} reduction/pH,^{25,26} enzyme/temperature,²⁷ light/pH,^{28,29} were developed.³⁰

Stimuli-responsive polymers are categorized into two types. The first type is characterized by a change in the equilibrium of the stimulus-responsive moiety.³¹ The second type is characterized by the cleavage of covalent chemical bonds upon stimuli. The former has the advantage to be reversible, and to respond more rapidly than the latter. The dual stimuli-responsive nanomedicines that have been developed to date undergo cleavage of covalent chemical bonds as a response to at least one of both stimuli and to the best of our knowledge, double equilibrium changing stimuli-responsive micelles have never been reported. In the present study, we developed dual temperature- and pH-responsive polymeric micelles based on reversible- and rapid-phase transition polymer blocks. These polymeric micelles were applied for a selective intracellular uptake in solid tumor cells upon external local heating, and an effective intracellular release of the anti-tumor agent at internal endosomal pH (Scheme 1).

The amphiphilic diblock copolymer comprises temperature-responsive corona segments of poly(*N*-isopropylacrylamide-*co*-

N,N-dimethylacrylamide) P(*N*IPAAm-*co*-DMAAm), and a pH-responsive core segment of poly[2-(diisopropylamino)ethyl methacrylate] (PDPA). This diblock copolymer forms a core-shell type polymeric micelle in water, which can encapsulate the hydrophobic anti-tumor agent doxorubicin (DOX). This polymeric micelle was characterized for their temperature-, and pH-responsive, hydrodynamic diameters, and critical micelle concentrations. The efficacy of polymeric micelles in anti-tumor agent delivery is evaluated in human cervical cancer HeLa cells.

Experimental section

Materials

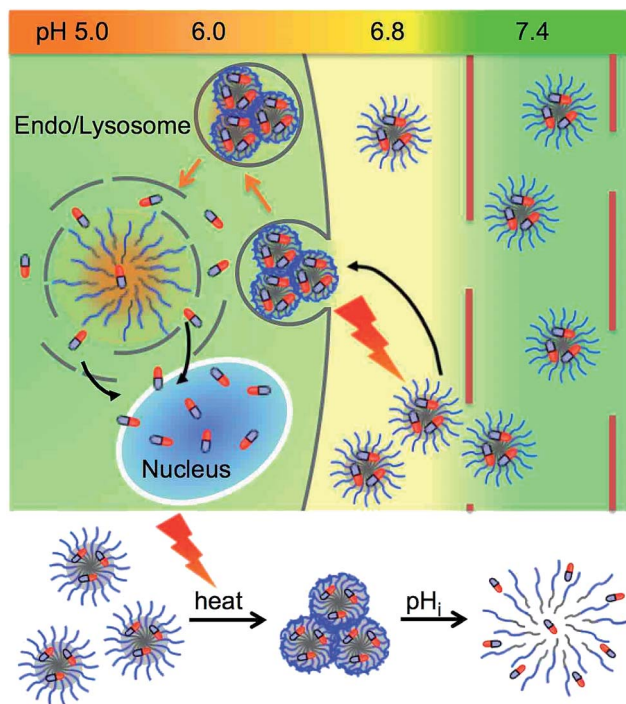
N-Isopropylacrylamide (NIPAAm) provided by KJ Chemicals Co. (Tokyo, Japan) was purified by recrystallization from *n*-hexane and dried at 25 °C *in vacuo*. Butyl methacrylate (BMA), *N,N*-dimethylacrylamide (DMAAm), 2,2'-azobisisobutyronitrile (AIBN), 2-aminoethanol, 1,4-dioxane, and dimethylformamide (DMF) were purchased from Wako Pure Chemical Industries Ltd (Osaka, Japan). BMA and DMAAm were distilled under reduced pressure before use. AIBN was recrystallized from methanol. 2-Cyano-2-propyl benzodithioate (CPBD), 2-(diisopropylamino)ethyl methacrylate (DPA) were purchased from Sigma-Aldrich (St. Louis, MO, USA). DPA passed through a neutral alumina column before use. Doxorubicin hydrochloride (DOX·HCl), and 5-dimethylthiazol-2-yl)-2,5-diphenyl tetrazolium bromide (MTT) were purchased from Tokyo Kasei Industry (Tokyo, Japan). Dialysis membranes [Spectra/Por 2 or 3, molecular weight cut-off (MWCO) 12–14 kDa and 3500 Da] were purchased from Spectrum Laboratories (Rancho Dominguez, CA, USA). Fetal bovine serum (Central America production, USDA approved) was purchased from Biosera (Kansas City, MO, USA).

Synthesis of poly[2-(diisopropylamino)ethyl methacrylate] (PDPA)

DPA (2.00 g, 9.41 mmol), and CPBD (86 mg, 0.39 mmol) as the RAFT chain transfer agent (CTA), AIBN (14 mg, 0.085 mmol) as a radical initiator, and the internal standard of 1,3,5-trioxane (one thirty weight of monomers) were dissolved in 3 mL 1,4-dioxane. The reaction mixture was degassed by a bubbling with nitrogen for 30 min, and after heating it to 70 °C for 20 h. The reaction solution was poured into methanol to precipitate the polymer, followed by drying to afford a pink solid. DPA conversion rate was 99%.

Synthesis of poly(butyl methacrylate) (PBMA)

BMA (2.00 g, 14.1 mmol), and CPBD (84 mg, 0.38 mmol) as the RAFT-CTA, AIBN (14 mg, 0.085 mmol) as a radical initiator, and the internal standard of 1,3,5-trioxane (one thirty weight of monomers) were dissolved in 4 mL 1,4-dioxane. The reaction mixture was degassed by a bubbling with nitrogen for 30 min, and after heating it to 70 °C for 20 h. The reaction solution was poured into methanol to precipitate the polymer, followed by drying to afford a pink solid. BMA conversion rate was 98%.



Scheme 1 Schematic illustration of temperature-responsive intracellular uptake, and pH-responsive drug release mechanism of drug loaded dual temperature- and pH-responsive polymeric micelle.



Diblock copolymerization of poly(NIPAAm-co-DMAAm) with PDPA (PDP-*b*-ND)

NIPAAm (1.21 g, 10.7 mmol), and DMAAm (0.458 g, 4.62 mmol) were dissolved in 4 mL 1,4-dioxane. Then, AIBN (3.1 mg, 0.019 mmol) as a radical initiator, PDPA (0.500 g, 0.0939 mmol) as MacroCTA, and the internal standard of 1,3,5-trioxane (one thirty weight of monomers) were added to the solution. The reaction mixture was degassed by a bubbling with nitrogen for 30 min, and after heating it to 70 °C. After reacting for 20 h, the reaction solution was poured into hexane : diethylether = 4 : 1 to precipitate the polymer. The crude was further purified by repeated precipitation from an acetone solution into hexane : diethylether = 4 : 1, followed by drying to afford a pale pink solid. NIPAAm, and DMAAm conversion rate were 57%, and 67%, respectively.

This solid (800 mg) was dissolved in 50 mL ethanol. Then, AIBN (149 mg, 0.907 mmol) was added to the solution. The reaction mixture was degassed by a bubbling with nitrogen for 30 min, and after heating to 80 °C. After reacting for 15 h, the solvent was evaporated and the resulting residue was dialyzed against methanol, and finally deionized water using dialysis membranes (MWCO 3500 Da) at room temperature. The obtained micelles solution was freeze-dried.

Diblock copolymerization of poly(NIPAAm-co-DMAAm) with PBMA (PBM-*b*-ND)

NIPAAm (1.10 g, 9.72 mmol), DMAAm (0.441 g, 4.45 mmol) were dissolved in 5 mL 1,4-dioxane. Then, AIBN (3.1 mg, 0.019 mmol) as a radical initiator, PBMA (0.502 g, 0.0930 mmol) as MacroCTA, and the internal standard of 1,3,5-trioxane (one thirty weight of monomers) were added to the solution. The reaction mixture was degassed by a bubbling with nitrogen for 30 min, and after heating it to 70 °C. After reacting for 20 h, the reaction solution was poured into hexane : diethylether = 4 : 1 to precipitate the polymer. The crude was further purified by repeated precipitation from an acetone solution into hexane : diethylether = 4 : 1, followed by drying to afford a pale pink solid. NIPAAm, and DMAAm conversion rate were 55%, and 65%.

This solid (800 mg) was dissolved in 50 mL ethanol. Then, AIBN (149 mg, 0.907 mmol) was added to the solution. The reaction mixture was degassed by a bubbling with nitrogen for 30 min, and after heating to 80 °C. After reacting for 15 h, the solvent was evaporated and the resulting residue was dialyzed against methanol, and finally deionized water using dialysis membranes (MWCO 3500 Da) at room temperature. The obtained micelles solutions were freeze-dried.

Characterization of polymers

¹H NMR spectra were recorded at 400 MHz on an Agilent 400-MR spectrometer. The monomer conversions of each reaction were determined by ¹H NMR analysis. For the conversion rate calculation, 1,3,5-trioxane peak was compared to the unreacted monomer peaks. The molecular weight of the polymer was determined by Gel Permeation Chromatography (GPC) analysis (GPC-8020 system; column, one TSKgel guardcolumn α and two TSKgel α -M connecting in a series; mobile phase, DMF

containing 10 mM LiCl; TOSOH, Tokyo, Japan), calibrated with polyethylene oxide standards.

Characterization of polymeric micelles

The obtained micelles powders were dissolved in aqueous buffer solutions. The LCST of polymeric micelles as a function of pH were determined by measuring the optical transmittance of its aqueous buffer solution (0.1 w/v%). The optical transmittance of the polymer solution was measured at 500 nm at various temperatures using a UV-Vis spectrophotometer (V-630, JASCO, Tokyo, Japan) and a PT-31 Peltier system (KRÜSS, Hamburg, Germany); the heating rate was 0.1 °C min⁻¹. The LCST was determined as the temperature at 50% of the optical transmittance of the polymer solution. In the case of reversible temperature-responsiveness evaluation, optical transmittances were measured after 30 seconds temperature was changed. The hydrodynamic diameters of polymeric micelles were determined using dynamic light scattering (Zetasizer Nano Series, Malvern Instrument Ltd., Malvern, UK). Zeta potential was measured using a zeta potential analyzer (ELSZ-2KOP, Otsuka Electronics Co., Ltd., Osaka, Japan). Fluorescence spectra of pyrene were recorded by a FP-6300 spectrofluorometer (JASCO) with the excitation wavelength 339 nm at 37 °C for the determining critical micelle concentration (CMC) of polymeric micelles. Pyrene was dissolved in acetone (100 μ M), and 5 μ L pyrene solution was added into 2 mL aqueous micelle solution with various concentrations. The fluorescence emission intensities at 373 and 383 nm were monitored.

Preparation of DOX loading polymeric micelles

DOX was loaded into polymeric micelles by the dialysis method. 40 mg diblock copolymer, 4 mg DOX·HCl, 10 μ L triethyl amine were dissolved in 2 mL DMF, and then the solutions were stored for 3 h at room temperature. DOX was neutralized with triethylamine. After 2 mL deionized water was then slowly added into the DMF solution under vigorous stirring, and then the solution was dialyzed against deionized water using dialysis membranes (MWCO 12–14 kDa), and finally dialysis was continued until no DOX leakage. DOX concentration was measured based on the absorbance intensity of DOX at 480 nm using a UV-Vis spectrophotometer. The drug loading content (DLC) and drug loading efficiency (DLE) were calculated using the following equations:

$$\text{DLC (\%)} = (\text{weight of loaded DOX} / \text{weight of DOX loaded NPs}) \times 100\%$$

$$\text{DLE (\%)} = (\text{weight of loaded DOX} / \text{weight of DOX in feed}) \times 100\%$$

Nile red assay

The pH-responsive drug release behavior of PDP-*b*-ND, and PBM-*b*-ND micelles was proved by Nile red assay. To examine the pH-dependent dye release, 100 μ L of Nile red loaded micelle solutions (4 mg mL⁻¹) were incubated in 1.9 mL of 5 mmol L⁻¹



$\text{Na}_2\text{HPO}_4/\text{NaH}_2\text{PO}_4$ containing 150 mmol L^{-1} NaCl buffer solutions as a function of pH for 1 min, then, the fluorescence spectra (from 550 nm to 700 nm) were measured by a FP-6300 spectrofluorometer (JASCO) with the excitation wavelength 540 nm at 37°C .

Cell culture

Human cervical cancer HeLa cells (RIKEN BRC CELL BANK) were cultured as subconfluent monolayers in a 100 mm culture dish in minimum essential medium Eagle (MEM) with non-essential amino acids (NEAA), supplemented with 10% fetal bovine serum (FBS), 50 units mL^{-1} of penicillin, and $50 \mu\text{g mL}^{-1}$ of streptomycin, in a humidified incubator at 37°C with 5% CO_2 .

Temperature-dependent intracellular uptake of DOX loaded polymeric micelles

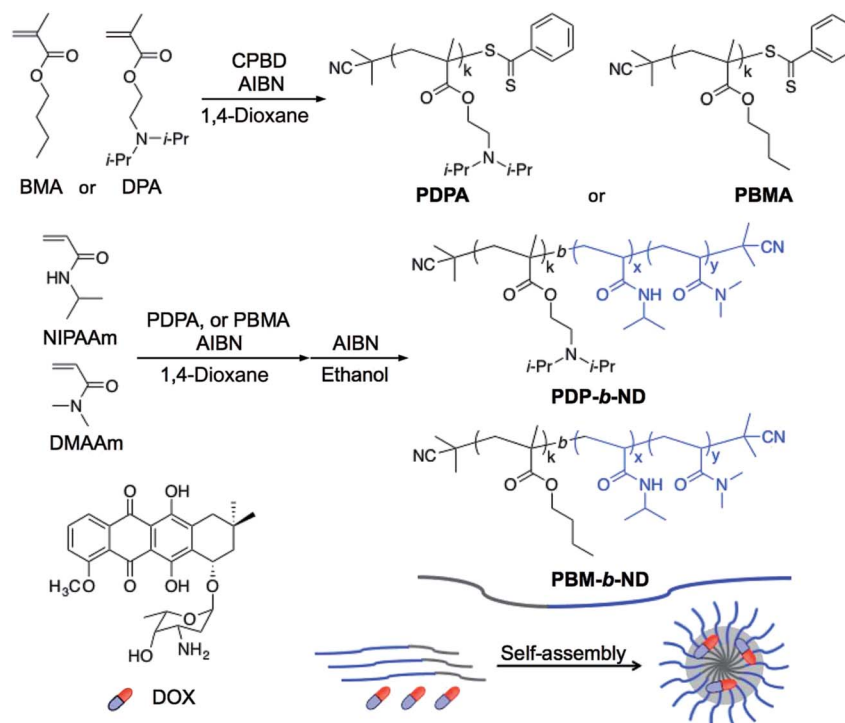
HeLa cells were seeded into 35 mm glass bottom dishes (5×10^4 cells, 2 mL per dish) and cultured for 1 day at 37°C in MEM with NEAA supplemented with 10% FBS in a humidified atmosphere containing 5% CO_2 . Cultured cells were exposed to DOX loaded **PDP-*b*-ND**, or **PBM-*b*-ND** ($100 \mu\text{g mL}^{-1}$) in MEM with 10% FBS at 37°C or at 42°C for 2 h with 5% CO_2 . After incubation, HeLa cells were rinsed once with a DPBS (–) buffer. For observing subcellular distribution, HeLa cells were seeded according to the description mentioned above. After incubation with **PDP-*b*-ND**, or **PBM-*b*-ND** ($10 \mu\text{g mL}^{-1}$) for 2 h at 42°C , HeLa cells were rinsed once with a DPBS (–) buffer and incubated for another 15 min with LysoTracker® Green (Invitrogen, $1.5 \mu\text{M}$), and cell nuclei staining

Hoechst 33342 (Invitrogen, 1 mg mL^{-1}) in MEM followed by rinsing once with DPBS (–). Samples were visualized with glass bottom dishes using a BZ-9000 microscope (Keyence, Osaka, Japan).

Cytotoxicity assay

The cytotoxicity to HeLa cells was evaluated by MTT assay. HeLa cells were seeded in a 24-well plates (1×10^4 cells, 500 μL per well) and cultured for 1 day at 37°C in MEM with NEAA supplemented with 10% FBS in a humidified atmosphere containing 5% CO_2 . Cultured cells were exposed to DOX loaded **PDP-*b*-ND**, and **PBM-*b*-ND** in MEM with 10% FBS at 37°C or at 42°C for 2 h with 5% CO_2 . After incubation, HeLa cells were rinsed twice with a DPBS (–) buffer. The medium replaced with 500 μL of fresh MEM with 10% FBS. After incubation for another 46 h, medium was replaced with 500 μL of fresh MEM with 5 mg mL^{-1} MTT in PBS (finally diluted to $500 \mu\text{g mL}^{-1}$). After incubation for an additional 2 h, 500 μL of the extraction buffer (acidified isopropanol) was added to the wells and the plate was shaken carefully. The absorbance of the solution was measured at 570 nm, and 630 nm (reference) by TECAN Infinite M1000 plate reader. The relative percentage of cell survival was calculated based on the 100% arbitrary absorbance obtained for the blank control. Reported values represent the mean standard deviation of 3 replicates on the same plate.

When evaluating the cytotoxicity of blank polymeric micelles, cultured cells were exposed to DOX free **PDP-*b*-ND**, and **PBM-*b*-ND** for 4 h at 42°C followed for 44 h at 37°C without



Scheme 2 Synthesis of PDPA, PBMA, PDP-*b*-ND and PBM-*b*-ND. Amphiphilic diblock copolymers formed core-shell type polymeric micelles with self-assembly, and encapsulated DOX in hydrophobic core.



medium change, then, MTT assay was performed in the same procedure above.

Results and discussion

Design and synthesis of dual temperature- and pH-responsive polymeric micelle

A pH-responsive core block **PDPA** was synthesized by RAFT polymerization using CPBD as a chain transfer agent (CTA). Amino groups have been incorporated into the polymers and were imparted a positive charge with decreasing pH, which induced the polymer chain to change from hydrophobic to hydrophilic. When a pH-responsive polymer with amino groups was applied to the core segment, the neutral amphiphilic diblock copolymer self-assembled with hydrophobic core at higher pH, whereas decreasing the pH led to the protonation of the core segment (hydrophilic) and induced fast disassembly of the micelle.³² The pH range, in which **PDPA** is responsive, is suitable for the disruption of micelles in acidic endo-/lysosomes and promotes drug release from the endocytosed drug carriers. A neutral hydrophobic core block **PBMA** was also synthesized with the same procedure as was used for the synthesis of **PDPA**. Next, the temperature-responsive corona segment P(NIPAAm-co-DMAAm) was synthesized by RAFT polymerization using **PDPA** or **PBMA** as macro-CTA. The dithiobenzoate end-group derived from the RAFT reagents was removed *via* radical-induced ester exchange.³³ PNIPAAm exhibits a temperature-dependent phase transition at its lower critical solution temperature (LCST),³⁴ which can be accurately raised to a slightly higher temperature than body temperature with hydrophilic co-monomers,³⁵ and intracellular uptake of PNIPAAm-based polymers, and nanomaterials can be controlled with temperature-dependent hydrophilic/hydrophobic phase transition.^{17,36,37} The two diblock copolymers, obtained using **PDPA** and **PBMA** as CTA, were referred to as **PDP-*b*-ND** and **PBM-*b*-ND**, respectively (Scheme 2). The number- and weight-averaged molecular weight (M_n , and M_w) and ratio of the two synthesized polymers were analyzed by ¹H NMR and gel-permeation chromatography (GPC), as shown in Table 1. In the case of ¹H NMR analysis, the molecular weights, and copolymer compositions were calculated with monomer conversions. ¹H NMR spectra of **PDPA**, **PBMA**, **PDP-*b*-ND**, and **PBM-*b*-ND** were shown in the ESI.† The copolymerization of two diblock polymers was confirmed by significant increase in molecular weight with GPC analysis.

These amphiphilic diblock copolymers formed core-shell type polymeric micelles in aqueous solution *via* the self-assembly of core segments, which can encapsulate hydrophobic DOX in their hydrophobic core. **PDP-*b*-ND** was designed to achieve a two-step DOX delivery with selective intracellular uptake *via* local tumor heating, and an effective release at acidic endo-/lysosomal pH with each of the segments responding to the stimuli independently. This system enables drug delivery specifically to the solid tumor with minimum drug leakage. DOX contents of **PDP-*b*-ND**, and **PBM-*b*-ND** micelles were 3.8% and 4.3% with a drug-loading efficiency of 43.4% and 48.6%, respectively.

Characterization of dual temperature- and pH-responsive polymeric micelle

The temperature-dependent optical transmittances of the **PDP-*b*-ND** and **PBM-*b*-ND** solutions as a function of pH are shown in Fig. 1a and b. Sharp transmittance curves were observed for **PDP-*b*-ND** at pH 7.4 and 6.4, and for **PBM-*b*-ND** at all pH. Their LCSTs were between 38.5 °C and 39.0 and controlled to a temperature slightly higher than body temperature, adjusting the composition ratio of NIPAAm and DMAAm. In addition, their optical transmittances at 36–37 °C (below LCST) was 90–93%, which were relatively lower than optical transmittance at 36–37 °C of **PDP-*b*-ND** at pH 5.4, indicating light scattering with the polymeric micelle (the Tyndall effect). Indeed, intense light scattering of the incident laser could be clearly observed (Fig. 1c). These results indicated that the corona of polymeric micelles was hydrophilic at body temperature, whereas it was hydrophobic at a temperature higher than 39 °C. At 36–40 °C and at pH 5.4, the optical transmittance of **PDP-*b*-ND** was above 99% and a lower light scattering of the incident laser was observed (Fig. 1c). This means that the Tyndall effect of the **PDP-*b*-ND** micelles was weakened due to a transition from micelle to unimer state, which implies that the **PDPA** core moiety transitioned from a hydrophobic to a positively charged hydrophilic state with decreasing pH. This transition is probably at the origin of the broadened transmittance curve and elevated LCST (above 42 °C) of **PDP-*b*-ND** at pH 5.4. Since the **PDPA** moiety of **PDP-*b*-ND** is a macro terminal group of P(NIPAAm-co-DMAAm), a large LCST shift was observed with lowering pH, which is not surprising as the LCST can even be affected by small molecules as terminal group.³⁸

The temperature- and pH-dependent hydrodynamic diameter of **PDP-*b*-ND**, and **PBM-*b*-ND** were measured, and Fig. 1d

Table 1 Characterization of the synthesized polymers

| | Monomer units ^a | | | | $M_{n,NMR}^b$ | $M_{n,GPC}^c$ | M_w/M_n^d |
|------------------------|----------------------------|-----|--------|-------|---------------|---------------|-------------|
| | DPA | BMA | NIPAAm | DMAAm | | | |
| PDPA | 24 | — | — | — | 5300 | 3700 | 1.11 |
| PDP-<i>b</i>-ND | 24 | — | 72 | 36 | 17 000 | 19 000 | 1.38 |
| PBMA | — | 36 | — | — | 5400 | 4000 | 1.10 |
| PBM-<i>b</i>-ND | — | 36 | 70 | 37 | 17 000 | 16 800 | 1.35 |

^a Determined by ¹H NMR. ^b M_n determined by ¹H NMR. ^c M_n determined by GPC. ^d Estimated by GPC.



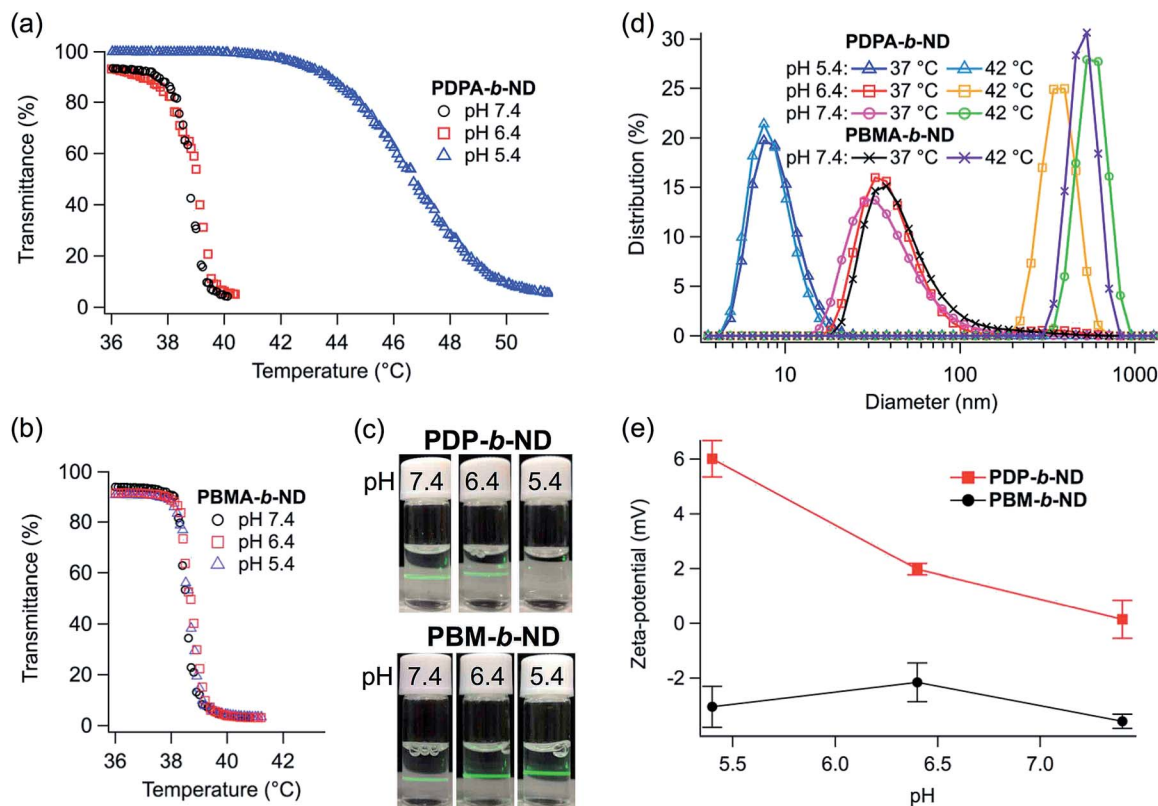


Fig. 1 Temperature-dependent optical transmittances of solutions at 500 nm at a heating rate of $0.1\text{ }^{\circ}\text{C min}^{-1}$. (a) **PDP-*b*-ND**, and (b) **PBM-*b*-ND**. (c) Photographs of **PDP-*b*-ND**, and **PBM-*b*-ND** with a green laser from the right hand side; $0.1\text{ w}/\%$ solutions in $5\text{ mmol L}^{-1}\text{ Na}_2\text{HPO}_4/\text{NaH}_2\text{PO}_4$ containing $150\text{ mmol L}^{-1}\text{ NaCl}$ at pH 7.4, 6.4, and 5.4. (d) Hydrodynamic diameters of **PDP-*b*-ND**, and **PBM-*b*-ND** ($200\text{ }\mu\text{g mL}^{-1}$) at pH 7.4, 6.4, and 5.4 in $5\text{ mmol L}^{-1}\text{ Na}_2\text{HPO}_4/\text{NaH}_2\text{PO}_4$ containing $150\text{ mmol L}^{-1}\text{ NaCl}$. (e) The zeta-potential of **PDP-*b*-ND**, and **PBM-*b*-ND** ($200\text{ }\mu\text{g mL}^{-1}$) in $5\text{ mmol L}^{-1}\text{ Na}_2\text{HPO}_4/\text{NaH}_2\text{PO}_4$. Error bars represent mean values $\pm 1\sigma$ ($n = 3$).

shows the size distributions as a function of pH at 37 and $42\text{ }^{\circ}\text{C}$. In the case of pH 7.4, and 6.4, the hydrodynamic diameters of the **PDP-*b*-ND** were around 50 nm, indicating that monodispersed micelles are formed at $37\text{ }^{\circ}\text{C}$, attributable to the hydrophilic corona. The hydrodynamic diameters increased to several hundred nm sizes at $42\text{ }^{\circ}\text{C}$, which is caused by the temperature-responsive corona of micelles changing from hydrophilic to hydrophobic characteristic, and subsequent aggregation by hydrophobic interactions between micelles. The temperature-responsive hydrodynamic size behaviors of **PBM-*b*-ND** were independent of the pH, and comparable to the behavior of **PDP-*b*-ND** at pH 7.4, and 6.4. At pH 5.4, the

hydrodynamic diameters were *ca.* 9 nm regardless of temperature, which supported that micelles of **PDP-*b*-ND** were broken down into individual polymers with lowering pH, as mentioned above. Moreover, the zeta-potential of **PDP-*b*-ND** increased from around 0 mV to positive ($\sim +6.0\text{ mV}$) with lowering pH. **PDPA** core was positively charged by protonation of (diisopropylamino)ethyl groups. In contrast, the zeta-potential of **PBM-*b*-ND** was slightly negative (around -3 mV), and did not appreciably change with pH values (Fig. 1e). Reversible temperature-responsiveness of **PDP-*b*-ND**, and **PBM-*b*-ND** at pH 7.4 were evaluated for three cycles between $37\text{ }^{\circ}\text{C}$ and $42\text{ }^{\circ}\text{C}$ as shown in Fig. 2. Reversible and fast phase transitions were clearly observed with temperature switching.

In order to investigate the disruption of **PDP-*b*-ND** micelles with lowering pH, critical micelle concentration (CMC) were evaluated from the fluorescence spectra of pyrene, used as hydrophobic fluorescence probe.³⁹ Once the polymeric micelle formed, pyrene molecules were preferentially incorporated into the hydrophobic core of the polymeric micelles and its fluorescence characteristic was changed drastically. Fig. 3a shows polymer concentration-dependent fluorescence intensity ratio (I_{373}/I_{383}) of pyrene. The CMC was estimated as the cross-point of two straight lines at low and high concentration regions. The CMC of **PDP-*b*-ND** at pH 7.4 was $7\text{ }\mu\text{g mL}^{-1}$, which increased to $159\text{ }\mu\text{g mL}^{-1}$ at pH 6.4, and was not observed (concentration <

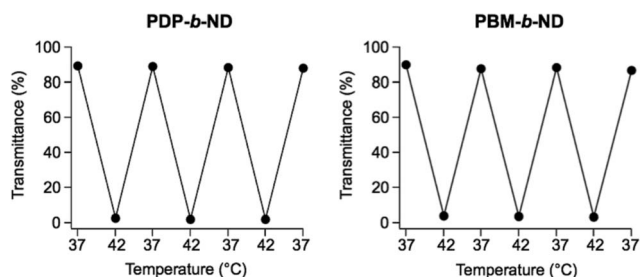


Fig. 2 Reversibility of temperature-dependent optical transmittances at 500 nm of **PDP-*b*-ND**, and **PBM-*b*-ND** solutions at pH 7.4. The temperatures were cyclically changed between $37\text{ }^{\circ}\text{C}$ and $42\text{ }^{\circ}\text{C}$.



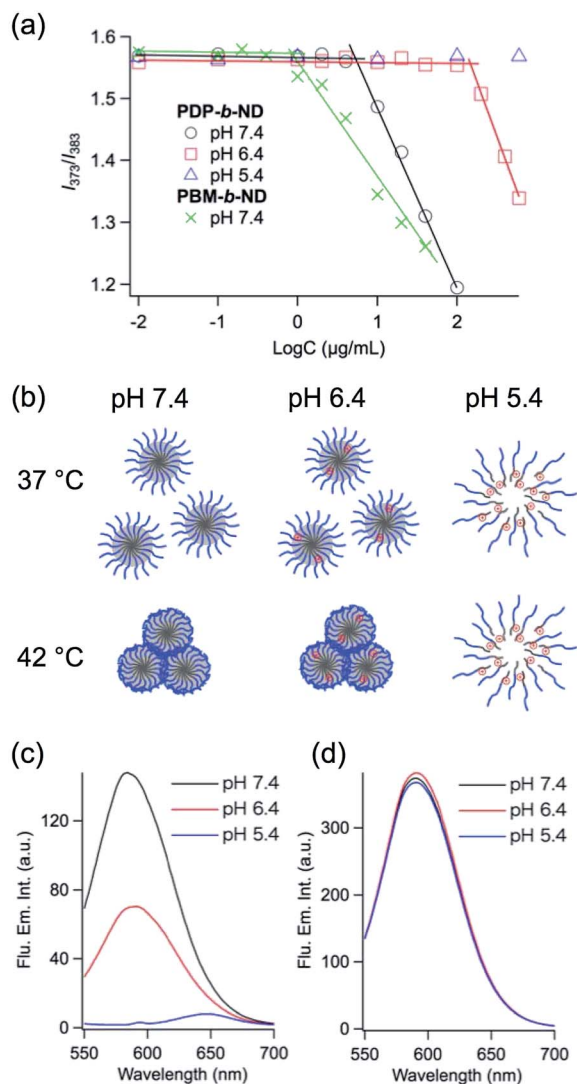


Fig. 3 (a) Block polymer concentration-dependent pyrene fluorescence emission ratios (I_{373}/I_{383}) in 5 mmol L⁻¹ Na₂HPO₄/NaH₂PO₄ containing 150 mmol L⁻¹ NaCl with **PDP-*b*-ND** at pH 7.4 (open circle), pH 6.4 (open square), pH 5.4 (open triangle), and **PBM-*b*-ND** at pH 7.4 (cross mark) at 37 °C. The concentration of pyrene is 0.25 μM ; the samples were excited at 339 nm. (b) Schematic illustration of **PDP-*b*-ND** micelles as a function of temperature and pH. Fluorescence emission spectra in function of the pH of Nile red (excited at 540 nm) encapsulated in (c) **PDP-*b*-ND** and (d) **PBM-*b*-ND** in 5 mmol L⁻¹ Na₂HPO₄/NaH₂PO₄ solution containing 150 mmol L⁻¹ NaCl buffer after incubation for 1 min.

600 $\mu\text{g mL}^{-1}$) at pH 5.4. These results indicated that **PDP-*b*-ND** micelle at physiological pH is transformed to unimer state with lowering pH. The CMC of **PBM-*b*-ND** micelle was 1 $\mu\text{g mL}^{-1}$, regardless of the pH, and was slightly lower than the CMC value of **PDP-*b*-ND**. The **PBMA** core moiety of **PBM-*b*-ND**, which was more hydrophobic than the **PDPA** core moiety of **PDP-*b*-ND**, formed stable micelles. The state of **PDP-*b*-ND** depending on temperature and pH is summarized in Fig. 3b.

Nile red is a fluorescent probe whose fluorescence is strongly influenced by the polarity of its environment, and inherently

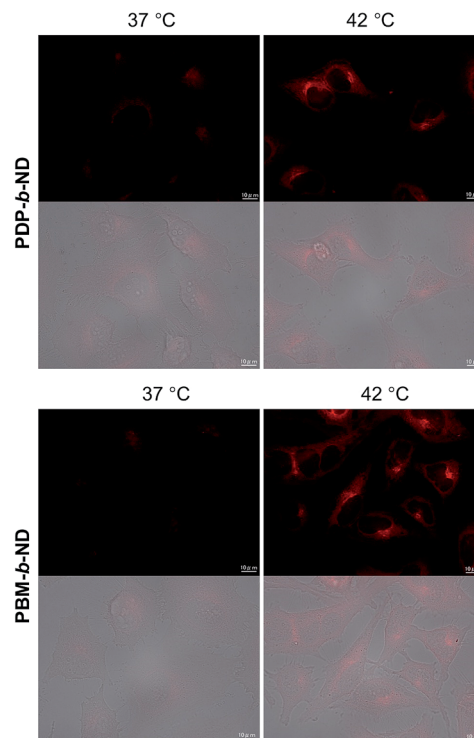


Fig. 4 Fluorescence microscopy images (upper panels) and overlays of fluorescence and phase contrast images (lower panels) of HeLa cells incubated with DOX-loaded **PDP-*b*-ND**, and **PBM-*b*-ND** for 2 h at 37 °C and 42 °C. Scale bar: 10 μm .

insoluble in water. Once Nile red as a hydrophobic model drug was embedded in hydrophobic core of micelles, it had strong fluorescence, whereas fluorescence was very weak after the release to aqueous medium from micelle. Therefore, the Nile red assay is a sensitive and convenient method to test the release behavior of nanomaterials.^{40,41} Fig. 3c and d show fluorescence emission spectra of Nile red encapsulated in **PDP-*b*-ND**, and **PBM-*b*-ND** micelles (200 $\mu\text{g mL}^{-1}$) as a function of pH after incubation for 1 min. In the case of **PBM-*b*-ND** solutions, fluorescence spectra with maximum emission at 590 nm were observed, and fluorescence intensities were independent of pH. On the other hand, fluorescence intensities in **PDP-*b*-ND** micelles were decreasing and undergoing a small red shift (pH 7.4 : 584 nm, pH 6.4 : 591 nm, and pH 5.4 : 647 nm) from pH 7.4 to pH 5.4. Because Nile red is a solvatochromic fluorescent dye,⁴² which shows a red shift with increasing polarity, these results indicated that Nile red was quickly (within 1 min) released with the burst of **PDP-*b*-ND** with lowering pH. In the case of stimuli-sensitive cleavage of covalent bond types, drug release times were rather long (up to hours).^{23–29} This result of **PDP-*b*-ND** micelles is favorable to endosomal escape.

The temperature-dependent cellular uptake of dual temperature- and pH-responsive polymeric micelle

The temperature-dependent intracellular uptake of DOX-loaded **PDP-*b*-ND** and **PBM-*b*-ND** micelles was evaluated using human cervical cancer HeLa cells at 37 °C and at 42 °C, the temperature at which local heating cancer therapy is conducted. Red



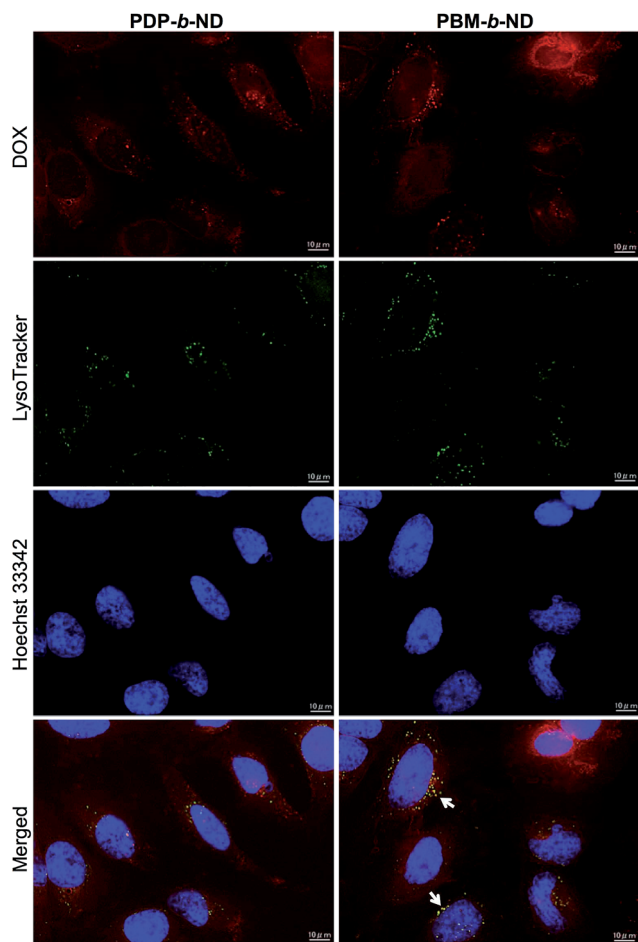


Fig. 5 Fluorescence microscopy images of HeLa cells incubated with DOX-loaded **PDP-*b*-ND**, and **PBM-*b*-ND** (red) for 2 h at 42 °C, endosome-specific LysoTracker (green), nuclei staining Hoechst 33342, and merged images. Scale bar: 10 μm.

fluorescence derived from DOX was clearly observed upon incubation at 42 °C, compared with incubation at 37 °C with both micelles, as shown in the fluorescence microscopy images in Fig. 4. In our previous work,³⁷ temperature-responsive polymeric nanoparticles with a P(NIPAAm-*co*-DMAAm) polymer brush attached on its surface showed a temperature-dependent cellular uptake, with its LCST as boundary. In accordance to our previous study, the temperature-responsive **PDP-*b*-ND** and **PBM-*b*-ND** micelles, which encapsulate DOX, were internalized into cells in a temperature-dependent manner, as they also have a P(NIPAAm-*co*-DMAAm) corona.

The localization of DOX-loaded **PDP-*b*-ND** and **PBM-*b*-ND** was visualized by co-staining with lysosome-specific LysoTracker green, and cell nuclei staining Hoechst 33342 as shown in Fig. 5. In the case of DOX-loaded **PBM-*b*-ND**, the red fluorescence derived from DOX was predominantly merged with the green dot fluorescence corresponding to LysoTracker green. On the other hand, in the case of DOX-loaded **PDP-*b*-ND**, the red fluorescence was rarely merged with the green dot. These results indicated that the endosomal escape of DOX-loaded

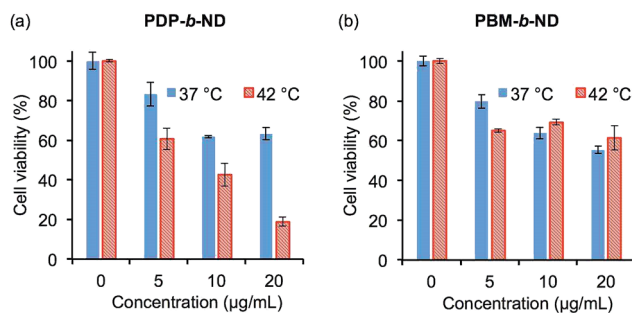


Fig. 6 Concentration-dependent viability of HeLa cells after incubation DOX-loaded (a) **PDP-*b*-ND**, and (b) **PBM-*b*-ND** for 2 h at 37 °C, and 42 °C. Cell viabilities were measured after 46 h treatment. Error bars represent mean values $\pm 1\sigma$ ($n = 3$).

PDP-*b*-ND was accelerated with the disruption by endosomal acidic pH, which triggered rapid DOX release to cytoplasm.

The temperature-dependent antitumor effect of DOX loaded dual temperature- and pH-responsive polymeric micelle

The temperature-dependent cytotoxicity of DOX-loaded and unloaded **PDP-*b*-ND** and **PBM-*b*-ND** micelles was evaluated using the MTT assay. As shown in Fig. 6a, significant greater cytotoxicity was observed with exposure to DOX-loaded **PDP-*b*-ND** at 42 °C compared to exposure at 37 °C. These results indicated that intracellular uptake of DOX encapsulated in **PDP-*b*-ND** was enhanced above LCST of **PDP-*b*-ND**, and correlated with the results of fluorescence microscopy imaging (Fig. 4). On the other hand, no significant temperature-dependent cytotoxicity was observed with exposure to DOX-loaded **PBM-*b*-ND**, regardless of temperature (Fig. 6b), although significant difference of intracellular uptake between exposure temperatures at 37 and 42 °C was observed with fluorescence microscopy imaging. The different cytotoxicity between **PDP-*b*-ND**, and **PBM-*b*-ND** micelles was due to the pH-responsive core moiety. The endocytosed **PDP-*b*-ND** micelles were disrupted with endosomal acidic pH, which triggered rapid DOX release, whereas the drug release from **PBM-*b*-ND** depended only on diffusion from the hydrophobic **PBMA** core. The blank polymeric micelles ($\sim 400 \mu\text{g mL}^{-1}$) showed no significant cytotoxicity with a HeLa cell viability of $>94\%$ even when combined with temperature treatment, indicating the biocompatibility of micelles (Fig. S1 in the ESI†). It was inferred that DOX-loaded **PDP-*b*-ND** micelles with local heating treatment have the potential to achieve efficient anti-tumor effect with regression of side effect.

Conclusions

In summary, we have developed dual temperature- and pH-responsive polymeric micelles, **PDP-*b*-ND** encapsulating DOX for selective and efficient cancer treatment. The hydrophilic/hydrophobic phase transition temperature of **PDP-*b*-ND** micelles with physiological pH was controlled to slightly higher than body temperature by the P(NIPAAm-*co*-DMAAm)



copolymer composition ratio of the temperature-responsive segment in the amphiphilic diblock copolymer. This characteristic enabled the suppression of intracellular uptake with body temperature, and the enhancement of intracellular uptake with local heating. In addition, **PDP-*b*-ND** micelles, internalized into the cell *via* endocytosis, were disrupted with acidic endosomal pH, which led to an effective release of the encapsulated DOX into the cell. Such dual responsive polymeric micelles, based on an equilibrium-changing stimuli-responsive system have not been generated previously, and are believed to achieve simultaneously solid tumor selective uptake and rapid release of encapsulated drug. Significant enhanced intracellular uptake of DOX at 42 °C was observed, while limited uptake was observed at body temperature with fluorescence microscopy. In addition, significant cytotoxicity of DOX-loaded **PDP-*b*-ND** at 42 °C was observed, compared to 37 °C. On the other hand, the cytotoxicity of DOX-loaded **PBM-*b*-ND** was independent of temperature, and lower than the cytotoxicity of DOX-loaded **PDP-*b*-ND**. These results indicated that the synergistic two-step delivery system with the enhancement of intracellular uptake with external thermal stimulation, and rapid release of DOX with internal acidic endosomal pH was effective to tumor treatment. This two-step drug delivery system demonstrates potential for tumor-specific chemotherapy with the combination of local hyperthermia.

Acknowledgements

This study was supported by Grant-in-Aid for Young Scientists (B) (Grant No. 15K18846) to YH from Japan Society for the Promotion of Science (JSPS), and The Research Foundation for Pharmaceutical Sciences to YH.

Notes and references

- 1 Y. Matsumura and H. Maeda, *Cancer Res.*, 1986, **46**, 6387.
- 2 H. Maeda, J. Wu, T. Sawa, Y. Matsumura and K. Hori, *J. Controlled Release*, 2000, **65**, 271–284.
- 3 A. Kolate, D. Baradia, S. Patil, I. Vhora, G. Kore and A. Misra, *J. Controlled Release*, 2014, **192**, 67–81.
- 4 K. Kataoka, A. Harada and Y. Nagasaki, *Adv. Drug Delivery Rev.*, 2001, **47**, 113–131.
- 5 H. Hatakeyama, H. Akita and H. Harashima, *Adv. Drug Delivery Rev.*, 2011, **63**, 152–160.
- 6 M. Wang and M. Thanou, *Pharmacol. Res.*, 2010, **62**, 90–99.
- 7 Y. Bae, W. D. Jang, N. Nishiyama, S. Fukushima and K. Kataoka, *Mol. Biosyst.*, 2005, **1**, 242–250.
- 8 Y. Miura, T. Takenaka, K. Toh, S. Wu, H. Nishihara, M. R. Kano, Y. Ino, T. Nomoto, Y. Matsumoto, H. Koyama, H. Cabral, N. Nishiyama and K. Kataoka, *ACS Nano*, 2013, **7**, 8583–8592.
- 9 J. Ahn, Y. Miura, N. Yamada, T. Chida, X. Liu, A. Kim, R. Sato, R. Tsumura, Y. Koga, M. Yasunaga, N. Nishiyama, Y. Matsumura, H. Cabral and K. Kataoka, *Biomaterials*, 2015, **39**, 23–30.
- 10 F. D. Jochum and P. Theato, *Chem. Soc. Rev.*, 2013, **42**, 7468–7483.
- 11 Y. Hiruta, Y. Nagumo, Y. Suzuki, T. Funatsu, Y. Ishikawa and H. Kanazawa, *Colloids Surf., B*, 2015, **132**, 299–304.
- 12 H. I. Lee, W. Wu, J. K. Oh, L. Mueller, G. Sherwood, L. Peteanu, T. Kowalewski and K. Matyjaszewski, *Angew. Chem., Int. Ed.*, 2007, **46**, 2453–2457.
- 13 Y. Hiruta, T. Funatsu, M. Matsuura, J. Wang, E. Ayano and H. Kanazawa, *Sens. Actuators, B*, 2015, **207**, 724–731.
- 14 H. Fu, D. M. Policarpio, J. D. Batteas and D. E. Bergbreiter, *Polym. Chem.*, 2010, **1**, 631–633.
- 15 P. Bawa, V. Pillay, Y. E. Choonara and L. C. d. Toit, *Biomed. Mater.*, 2009, **4**, 022001.
- 16 P. Wust, B. Hildebrandt, G. Sreenivasa, B. Rau, J. Gellermann, H. Riess, R. Felix and P. M. Schlag, *Lancet Oncol.*, 2002, **3**, 487–497.
- 17 J. Akimoto, M. Nakayama, K. Sakai and T. Okano, *Biomacromolecules*, 2009, **10**, 1331–1336.
- 18 F. Kohori, K. Sakai, T. Aoyagi, M. Yokoyama, M. Yamato, Y. Sakurai and T. Okano, *Colloids Surf., B*, 1999, **16**, 195–205.
- 19 D. E. Meyer, B. C. Shin, G. A. Kong, M. W. Dewhirst and A. Chilkoti, *J. Controlled Release*, 2001, **74**, 213–224.
- 20 M. Stubbs, P. M. J. McSheehy, J. R. Griffiths and C. L. Bashford, *Mol. Med. Today*, 2000, **6**, 15–19.
- 21 A. K. Varkouhi, M. Scholte, G. Storm and H. J. Haisma, *J. Controlled Release*, 2011, **151**, 220–228.
- 22 J. Liu, Y. Huang, A. Kumar, A. Tan, S. Jin, A. Mozhi and X. J. Liang, *Biotechnol. Adv.*, 2014, **32**, 693–710.
- 23 Y. Dong, J. Yang, H. Liu, T. Wang, S. Tang, J. Zhang and X. Zhang, *Theranostics*, 2015, **5**, 890–904.
- 24 J. Z. Du, X. J. Du, C. Q. Mao and J. Wang, *J. Am. Chem. Soc.*, 2011, **133**, 17560–17563.
- 25 M. Huang, K. Zhao, L. Wang, S. Lin, J. Li, J. Chen, C. Zhao and Z. Ge, *ACS Appl. Mater. Interfaces*, 2016, **8**, 11226–11236.
- 26 J. Li, Y. Han, Q. Chen, H. Shi, S. u. Rehman, M. Siddiq, Z. Ge and S. Liu, *J. Mater. Chem. B*, 2014, **2**, 1813–1824.
- 27 S. Kashyap, N. Singh, B. Surnar and M. Jayakannan, *Biomacromolecules*, 2016, **17**, 384–398.
- 28 Q. Jin, T. Cai, H. Han, H. Wang, Y. Wang and J. Ji, *Macromol. Rapid Commun.*, 2014, **35**, 1372–1378.
- 29 L. Meng, W. Huang, D. Wang, X. Huang, X. Zhu and D. Yan, *Biomacromolecules*, 2013, **14**, 2601–2610.
- 30 R. Cheng, F. Meng, C. Deng, H. A. Klok and Z. Zhong, *Biomaterials*, 2013, **34**, 3647–3657.
- 31 Y. Zhang, C. Wang, C. Xu, C. Yang, Z. Zhang, H. Yan and K. Liu, *Chem. Commun.*, 2013, **49**, 7286–7288.
- 32 K. Zhou, Y. Wang, X. Huang, K. Luby-Phelps, B. D. Sumer and J. Gao, *Angew. Chem., Int. Ed.*, 2011, **50**, 6109–6114.
- 33 S. Perrier, P. Takolpuckdee and C. A. Mars, *Macromolecules*, 2005, **38**, 2033–2036.
- 34 M. Heskins and J. E. Guillet, *J. Macromol. Sci., Chem.*, 1968, **2**, 1441–1455.
- 35 Y. Hiruta, M. Shimamura, M. Matsuura, Y. Maekawa, T. Funatsu, Y. Suzuki, E. Ayano, T. Okano and H. Kanazawa, *ACS Macro Lett.*, 2014, **3**, 281–285.
- 36 A. Yamada, Y. Hiruta, J. Wang, E. Ayano and H. Kanazawa, *Biomacromolecules*, 2015, **16**, 2356–2362.
- 37 Y. Hiruta, R. Nemoto and H. Kanazawa, *Colloids Surf., B*, 2017, **153**, 2–9.



Paper

- 38 Y. Hiruta, Y. Nagumo, A. Miki, T. Okano and H. Kanazawa, *RSC Adv.*, 2015, **5**, 73217–73224.
- 39 M. Wilhelm, C. L. Zhao, Y. Wang, R. Xu, M. A. Winnik, J. L. Mura, G. Riess and M. D. Croucher, *Macromolecules*, 1991, **24**, 1033–1040.
- 40 S. Tang, Q. Yin, Z. Zhang, W. Gu, L. Chen, H. Yu, Y. Huang, X. Chen, M. Xu and Y. Li, *Biomaterials*, 2014, **35**, 6047–6059.
- 41 J.-H. Ryu, R. T. Chacko, S. Jiwpanich, S. Bickerton, R. P. Babu and S. Thayumanavan, *J. Am. Chem. Soc.*, 2010, **132**, 17227–17235.
- 42 O. A. Kucherak, S. Oncul, Z. Darwich, D. A. Yushchenko, Y. Arntz, P. Didier, Y. Mély and A. S. Klymchenko, *J. Am. Chem. Soc.*, 2010, **132**, 4907–4916.

